

Accessible precisions for estimating two conjugate parameters using Gaussian probes

Syed M. Assad^{1,2,3,*}, Jiamin Li,¹ Yuhong Liu,¹ Ningbo Zhao,¹ Wen Zhao,¹ Ping Koy Lam,³ Z. Y. Ou,^{1,4,†} and Xiaoying Li^{1,‡}

¹College of Precision Instrument and Opto-Electronics Engineering, Key Laboratory of Opto-Electronics Information Technology, Ministry of Education, Tianjin University, Tianjin 300072, China

²School of Physical and Mathematical Sciences, Nanyang Technological University, 639673 Singapore

³Centre for Quantum Computation and Communication Technology, Department of Quantum Science, Research School of Physics and Engineering, Australian National University, Canberra ACT 2601, Australia

⁴Department of Physics, Indiana University-Purdue University Indianapolis, Indianapolis, Indiana 46202, USA



(Received 21 October 2019; revised manuscript received 16 March 2020; accepted 20 March 2020; published 18 May 2020)

We analyze the precision limits for a simultaneous estimation of a pair of conjugate parameters in a displacement channel using Gaussian probes. Having a set of squeezed states as an initial resource, we compute the Holevo Cramér-Rao bound to investigate the best achievable estimation precisions if only passive linear operations are allowed to be performed on the resource prior to probing the channel. The analysis reveals the optimal measurement scheme and allows us to quantify the best precision for one parameter when the precision of the second conjugate parameter is fixed. To estimate the conjugate parameter pair with equal precision, our analysis shows that the optimal probe is obtained by combining two squeezed states with orthogonal squeezing quadratures on a 50:50 beam splitter. If different importance is attached to each parameter, then the optimal mixing ratio is no longer 50:50. Instead, it follows a simple function of the available squeezing and the relative importance between the two parameters.

DOI: 10.1103/PhysRevResearch.2.023182

I. INTRODUCTION

How precise can we make a set of physical measurements? This is a fundamental question that has driven much of the progress in science and technology. Improving the precisions and understanding limitations to measurements have often led to revolutionary discoveries or new insights in science. After overcoming technical sources of noise, the presence of quantum noise imposes a limit to the ultimate measurement precision. Due to the presence of quantum fluctuations, estimation precision using classical probe fields is limited to the *standard quantum limit* for optical measurements. In order to surpass this limit, a quantum resource such as squeezed states [1–3] or entangled states [4–17] are required. A notable example is the use of quadrature squeezed states of light to enhance the detection of gravitational waves [18,19]. Another concept in quantum mechanics that distinguishes it from classical mechanics is that of noncommuting observables. This imposes a limitation for simultaneously estimating multiple parameters encoded in noncommuting observables.

In this work, we consider the problem of estimating two independent parameters $\theta = (\theta_x, \theta_y)$, encoded in two

conjugate quadratures X and Y of a displacement channel $D(\theta) = \exp(\frac{i\theta_y}{2}X - \frac{i\theta_x}{2}Y)$. This channel induces a displacement of θ_x on the amplitude quadrature X and θ_y on the phase quadrature Y of a single-mode optical field with $[X, Y] = 2i$. This problem has attracted a lot of attention since the early days of quantum mechanics [20–22] and continue to do so [11,14,23]. For example, if a single-mode probe is used to sense the displacement, the work by Arthurs and Kelly showed that the estimation mean squared errors v_x and v_y are bounded by $v_x, v_y \geq 4$ [20]. However, it was theoretically shown [16,24,25] and experimentally demonstrated [15,26,27] that by utilising quantum entanglement between two systems—for example, through the quantum dense coding scheme—it is possible to circumvent this limit and estimate both parameters with accuracies beyond the standard quantum limit.

More recently, the pioneering works by Holevo and Helstrom on quantum estimation theory [28–30] have been used to study this problem [11,13,14,31]. Once the probe state is specified, the quantum Fisher information determines a bound on the estimation precision thorough the quantum Cramér-Rao bound (CRB), which holds for every possible measurement strategy. There are many variants of the quantum CRB—the two most popular being the symmetric logarithmic derivative (SLD) [28,29,32,33] and the right logarithmic derivative (RLD) [33–38] as these yield direct bounds for the sum of the mean squared error. These have been widely used since they are relatively easy to compute [39,40]. For single-parameter estimation, the SLD-CRB offers an asymptotically tight bound on the precision [41]. However for multiparameter estimation, neither the SLD-CRB nor the RLD-CRB is neces-

*cqtsma@gmail.com

†zou@iupui.edu

‡xiaoyingli@tju.edu.cn

sarily tight [42,43]. Hence even though the probe might offer a large quantum Fisher information, their CRB might not be *achievable*, which means that the actual achievable precisions are not known.

Here, we solve this problem by using the Holevo Cramér-Rao bound to compute the actual asymptotically achievable precision [30,44–47]. Knowing the achievable precision for a specific probe allows us to compare metrological performances between two different probes. We can then use this formalism to answer the question: given a fixed quantum resource such as squeezing, how do we use it to optimally sense the channel? The resource states that we consider will be one-mode and two-mode Gaussian states, which we are allowed to freely mix or rotate before sending one mode to probe the channel. In doing so, we derive ultimate bounds on simultaneous parameter estimation which goes beyond existing restrictions imposed by the SLD or RLD-CRB. These bounds quantify a *resource apportioning principle*—the resource can be allocated to gain either a precise estimate of θ_x or θ_y but not both together [16,48].

The paper is organized as follows. We start with a summary of the general framework for two-parameter estimation in Sec. II. Next we apply this framework to derive from the Fisher information precision limits for a single mode probe in Sec. III. We then generalize this result to two-mode probes in Sec. IV. We show that at least 6 dB of squeezing is necessary to surpass the standard quantum limit. We also elucidate our results with two examples: the first with a single squeezed state and the second with two squeezed states with equal amount of squeezing. Finally, we end with some discussions in Sec. V.

II. GENERAL FRAMEWORK

Let us begin with a brief review of the two-parameter estimation problem and the Holevo Cramér-Rao bound. To estimate the parameters θ , the state ρ_0 is sent through the displacement channel $D(\theta)$ as a probe. After the interaction, the state becomes $\rho_\theta = D(\theta)\rho_0D(\theta)^\dagger$ which now contains information about the two parameters of interest. Next, we perform some measurement scheme and use an estimation strategy which leads to two unbiased estimators $\hat{\theta}_x$ and $\hat{\theta}_y$. We quantify the performance of these estimators, through the mean squared errors

$$v_x := \mathbb{E}[(\hat{\theta}_x - \theta_x)^2] \quad \text{and} \quad v_y := \mathbb{E}[(\hat{\theta}_y - \theta_y)^2]. \quad (1)$$

When restricted to classical probes, due to quantum noise we have $v_x \geq 1$ and $v_y \geq 1$ which is known as the standard quantum limit. The aim of this work is to find out what are the possible values that v_x and v_y can take simultaneously. To quantify the performance for estimating both θ_x and θ_y simultaneously, we use the weighted sum of the mean squared error: $w_x v_x + w_y v_y$ as a figure of merit where w_x and w_y are positive weights that quantify the importance we attach to parameters θ_x and θ_y , respectively. We want to find an estimation strategy that minimizes this quantity.

The Holevo-CRB sets an asymptotically attainable bound on the weighted sum of the mean squared error [30]

$$w_x v_x + w_y v_y \geq f_{\text{HCR}} := \min_{\mathcal{X}} h_\theta[\mathcal{X}], \quad (2)$$

where $\mathcal{X} = \{\mathcal{X}_x, \mathcal{X}_y\}$ are Hermitian operators that satisfy the locally unbiased conditions

$$\text{tr}\{\rho_\theta \mathcal{X}_j\}|_{\theta=0} = 0 \quad \text{and} \quad \text{tr}\left\{\frac{\partial \rho_\theta}{\partial \theta_j} \mathcal{X}_k\right\}|_{\theta=0} = \delta_{jk}, \quad (3)$$

for $j, k \in \{x, y\}$ and h_θ is the function

$$h_\theta[\mathcal{X}] := \text{Tr}\{W \text{Re}Z_\theta[\mathcal{X}]\} + \|\sqrt{W} \text{Im}Z_\theta[\mathcal{X}]\sqrt{W}\|_1. \quad (4)$$

Here, Z is the 2-by-2 matrix $Z_{jk} := \text{tr}\{\rho_\theta \mathcal{X}_j \mathcal{X}_k\}$ and W is a diagonal matrix with entries w_x and w_y . The bound depends on the state ρ_θ only; it does not need for us to specify any measurement. For quadrature displacements with Gaussian probes, the bound involves minimisation of a convex function over a convex domain. This is an instance of convex optimisation problem which can be calculated efficiently by numerical methods [14]. Furthermore, the optimisation also reveals an explicit measurement scheme that saturates the bound. For Gaussian probes, the optimal measurement will always be an individual Gaussian measurement.

III. PRECISION BOUNDS FOR SINGLE-MODE PROBE

We now apply the formalism to a pure single-mode amplitude squeezed state probe with quadrature variance e^{-2r} and rotated by an angle ϕ as shown in Fig. 1(a). The formal definitions for the rotation and squeezing operators are given in Appendix A. As previously stated, the Holevo-CRB only depends on the probe and how it varies with the parameters. In the single mode case, as shown in Appendix B, constraints (3) fully determines f_{HCR} . There is no free parameter in the optimisation and as a result, Holevo-CRB (2) becomes

$$w_x v_x + w_y v_y \geq w_x v_a + w_y v_b + 2\sqrt{w_x w_y}, \quad (5)$$

where

$$v_a := e^{-2r} \cos^2 \phi + e^{2r} \sin^2 \phi, \quad (6)$$

$$v_b := e^{-2r} \sin^2 \phi + e^{2r} \cos^2 \phi, \quad (7)$$

are the projected variances on the X and Y quadratures. For every choice of w_x/w_y , Eq. (5) defines a straight line in the v_x - v_y plane and gives a different bound on that plane. Some of these bounds are plotted in Fig. 1(b) for $e^{-2r} = 1/2$ and $\phi = \pi/6$. For example, to estimate both θ_x and θ_y with equal precision, setting $w_x = w_y = 1$ gives the best estimation strategy with $v_x + v_y = 2(1 + \cosh 2r)$ independent of ϕ . This gets worse with more squeezing. However, if we are only concerned with estimating θ_x , setting $w_y = 0$ results in $v_x = v_a$. By eliminating w_x and w_y from Eq. (5), we can collect all these bounds into one stricter bound

$$(v_y - v_b)(v_x - v_a) \geq 1 \quad (8)$$

which holds for every ϕ . This is plotted in Fig. 1(c) for a few values of ϕ . Every pair of (v_x, v_y) that satisfies Eq. (8) can be achieved by a specific measurement strategy. The same relation is plotted in Fig. 1(d) as a function of the precisions $1/v_x$ and $1/v_y$. This relation quantifies the resource apportioning principle—given a fixed amount of squeezing, there is only so much improvement in the precision to be had. The resource can be used to gain a precise estimate of θ_x , but this comes at the expense of an imprecise estimate of θ_y .

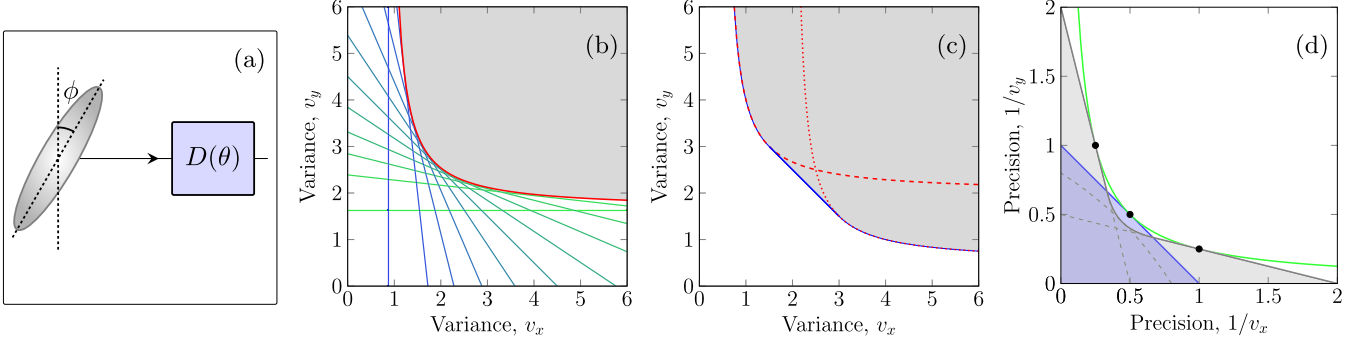


FIG. 1. (a) A squeezed state is used to sense the parameter θ of a displacement channel. (b) With 3 dB of squeezing, and for a fixed squeezing angle $\phi = \pi/6$, each of the straight line is the Holevo-CRB (5) with a different value of w_x/w_y . The shaded area shows the accessible variance for simultaneously estimating θ_x and θ_y . (c) The two red dashed and dotted lines can be achieved by an X and P squeezed state with $\phi = 0$ and $\pi/2$, respectively. The blue line requires an intermediate squeezing angle. The shaded area are all the accessible regions for a single mode squeezed state. (d) This shows the same region as (c) but as a function of the precision. With a 3 dB squeezed state, we can reach the grey areas. More squeezing can give a high precision for one parameter but at the expense of a lower precision for the other. The product of the precisions will never exceed 1/4 regardless of the squeezing level. This is shown as the green line. The three grey dashed lines plot Eq. (8) when the squeezing angles are fixed at $\phi = 0, \pi/4$, and $\pi/2$. The vacuum probe can only access the blue region.

When $\phi = 0$, relation (8) can be written concisely as a bound on the weighted sum of the precisions

$$\frac{e^{-2r}}{v_x} + \frac{e^{2r}}{v_y} \leq 1. \quad (9)$$

By using the arithmetic-geometric mean inequality, an immediate corollary of the result is the Arthurs and Kelly relation $v_x v_y \geq 4$ which holds for all r [16,20]. This reflects the Heisenberg uncertainty relation imposed on a single mode system. Every value of squeezing can saturate this inequality at one value of v_x and v_y as seen in Fig. 1(d). As we shall show next, this restriction can be somewhat relaxed using two mode states, but the sum of the precisions are still constrained by the total available resource.

IV. PRECISION BOUNDS FOR TWO-MODE PROBE

We now consider a two-mode system where we have access to two amplitude-squeezed states with quadrature variances e^{-2r_1} and e^{-2r_2} . Furthermore we are allowed to rotate them by ϕ_1 and ϕ_2 , and mix the two through a beam-splitter of transmissivity t before sending one mode through the displacement channel as shown in Fig. 2(a). In this case, f_{HCR} does not have a simple form; its computation involves finding the root of a quartic function. Despite this, the collection of all the bounds lead to a final expression that is surprisingly simple and intuitive. This is our main result: given two pure squeezed states with variances e^{-2r_1} and e^{-2r_2} as a resource where $0 \leq r_1 \leq r_2$, and allowing for rotation and mixing operations, the measurement sensitivity is limited by

$$v_y \geq v_y^* = \begin{cases} \frac{v_x e^{-2r_1}}{v_x - e^{-2r_2}} & \text{if } e^{-2r_2} \leq v_x < v_c \\ (e^{-r_1} + e^{-r_2})^2 - v_x & \text{if } v_c \leq v_x < v_d \\ \frac{v_x e^{-2r_2}}{v_x - e^{-2r_1}} & \text{if } v_d \leq v_x \end{cases}, \quad (10)$$

where $v_c := e^{-2r_2} + e^{-r_1-r_2}$ and $v_d := e^{-2r_1} + e^{-r_1-r_2}$. The full derivation requires a lengthy but straightforward

minimization and is done in Appendix C. It involves finding the optimal values of ϕ_1, ϕ_2 and t for every pair of w_x and w_y . We outline the main steps in the derivations here. Firstly, for a fixed value of w_x and w_y and t , we can numerically compute the Holevo-CRB for each pair of ϕ_1 and ϕ_2 . We find that the optimal setting for ϕ_2 is when $\phi_2 = \phi_1 + \pi/2$, making the two squeezed states as different as possible [49]. Secondly, for a fixed ϕ_1 and t , each pair of w_x and w_y gives a bound which correspond to one of the straight lines plotted in Fig. 2(b). The collection of all these bounds give the accessible region for this probe configuration. Thirdly, we vary t to find the accessible region for a fixed ϕ_1 as shown in Fig. 2(c). Finally the optimal value of ϕ_1 is determined to arrive at the final result (10).

The region described by (10) is plotted in Fig. 2(d). Every pair of (v_x, v_y) that satisfies relation (10) can be attained by a dual homodyne measurement. An immediate corollary of this is the relation $v_x v_y \geq 4e^{-2r_1} e^{-2r_2}$ [27]. In order to surpass the standard quantum limit for both parameters, we require $e^{-2r_1} e^{-2r_2} < 1/4$. In other words, the sum of the squeezed variances of the resource has to be greater than approximately 6 dB.

As mentioned in the outline of the derivations, not all regions in (10) can be reached using the same probe. Different region requires the resource to be used differently. For $w_x < w_y$, the best way to use the available resource is to set $\phi_1 = 0$ and $\phi_2 = \pi/2$ and mix them on a beam-splitter with transmissivity

$$t = \frac{e^{r_1}}{e^{r_1} + e^{r_2} \sqrt{w_x/w_y}}. \quad (11)$$

This gives the optimal variances

$$v_x = e^{-2r_1} + e^{-(r_1+r_2)} \sqrt{w_y/w_x}, \quad (12)$$

$$v_y = e^{-2r_2} + e^{-(r_1+r_2)} \sqrt{w_x/w_y}, \quad (13)$$

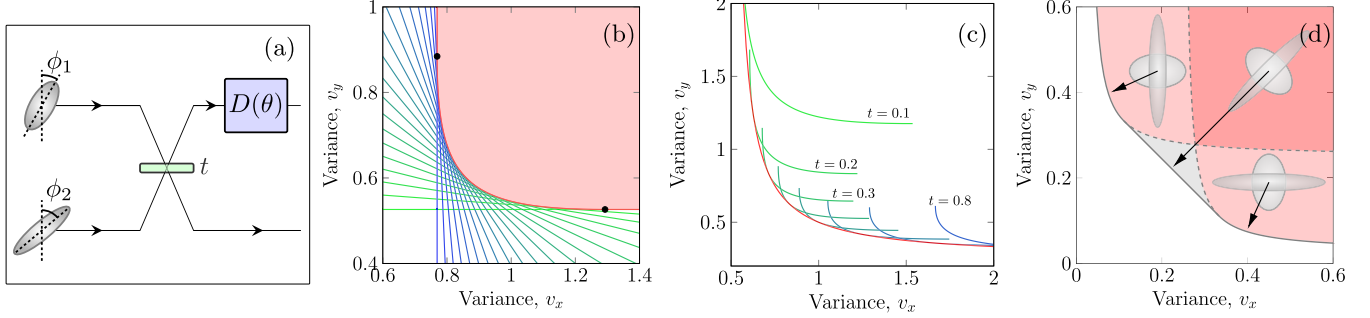


FIG. 2. (a) Two squeezed states are used to sense the displacement θ . (b) The Holevo-CR bound for a two-mode probe with $r_1 = 0.35$, $r_2 = 0.69$, $t = 0.4$, $\phi_1 = 0$, and $\phi_2 = \pi/2$. Each straight line correspond to a bound with different values of w_x/w_y . The pink region shows all the accessible values of v_x and v_y . (c) Each bluish-green curve gives the accessible boundary for the same probe as (b) except for the value of t which varies from 0.1 to 0.8 in steps of 0.1. The red curve is the envelope of all the blueish-green curve. (d) The shaded areas show the relation (10) having two squeezed probes with 6 and 15.6 dB of squeezing. The variance for estimating both parameters can be simultaneously smaller than 1. The two grey dashed lines are limits when the probe is fixed with $\phi_1 = 0$ and $\pi/2$ given by Eq. (15).

or in terms of t ,

$$v_x = \frac{e^{-2r_1}}{1-t} \text{ and } v_y = \frac{e^{-2r_2}}{t} \quad (14)$$

for $t > \frac{e^{r_1}}{e^{r_1} + e^{r_2}}$. After eliminating t , we arrive at a bound on the precisions

$$\frac{e^{-2r_1}}{v_x} + \frac{e^{-2r_2}}{v_y} \leq 1. \quad (15)$$

For $w_y < w_x$, we just need to swap the roles of x and y by setting $\phi_1 = \pi/2$ and $\phi_2 = 0$. Equations (11)–(15) still hold with all x and y swapped. When $w_x = w_y$, there is a family of estimation strategy that all give the same sum of variances $v_x + v_y = (e^{-r_1} + e^{-r_2})^2$ but different values for each individual variances. This can be accessed by varying ϕ_1 from 0 to $\pi/2$ with $\phi_2 = \phi_1 + \pi/2$ and keeping t as Eq. (11) which gives

$$\left. \begin{aligned} v_x \\ v_y \end{aligned} \right\} = \frac{1}{2}(e^{-r_1} + e^{-r_2})^2 \pm \frac{\cos 2\phi_1}{2}(e^{-2r_1} - e^{-2r_2}). \quad (16)$$

In the following, we illustrate these results with two examples. In these example, we present the optimal probe and measurement strategy that saturates the estimation precisions (10).

A. Example 1: One squeezed state and one vacuum

In our first example, we consider the case of one squeezed state and one vacuum state ($r_1 = 0$) as shown in Fig. 3 inset. For $w_x < w_y$, the optimal use of the probe is to set $\phi_2 = \pi/2$ and the optimal measurement setup is shown in Fig. 4. The two quadrature measurements give independent estimates of θ_x and θ_y with variances

$$v_x = \frac{1}{1-t} \text{ and } v_y = \frac{e^{-2r_2}}{t}. \quad (17)$$

For $\frac{1}{1+e^{r_2}} \leq t \leq 1$, this pair of variances is optimal. Eliminating t , we can improve on the single mode precision relation

(9) with

$$\frac{1}{v_x} + \frac{e^{-2r_2}}{v_y} \leq 1 \quad (18)$$

which is plotted as the dashed grey line in Fig. 3 for $e^{-2r_2} = 1/4$. For example, it is possible to have $v_x = 2e^{-2r_2}$ and $v_y = 2$ where the product $v_x v_y = 4e^{-2r_2}$. If the resource variance $e^{-2r_2} < 1/4$ (greater than 6 dB), then $v_x v_y < 1$, surpassing what is sometimes called the standard quantum limit.

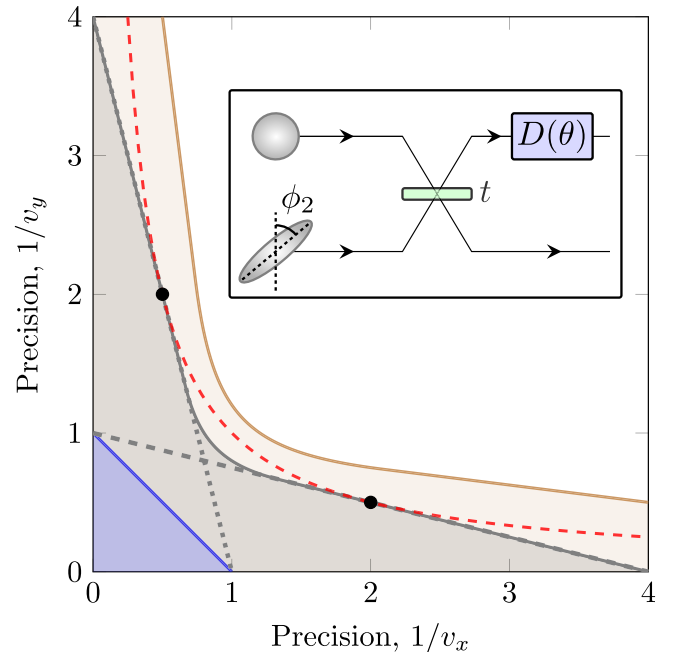


FIG. 3. In order to surpass the standard quantum limit, $v_x v_y = 1$ (red dashed line), we require access to an additional ancillary mode. The accessible region for a squeezed state with 6 dB of squeezing is shown as the grey shaded region. It can just reach the standard quantum limit at the two black dots. The dashed and dotted grey lines plot Eqs. (18) and (20) which can be accessed by setting $\phi_2 = \pi/2$ and $\phi_2 = 0$ respectively. With 9 dB of squeezing, we can clearly surpass this limit (brown region). These bounds are given by Eq. (10).

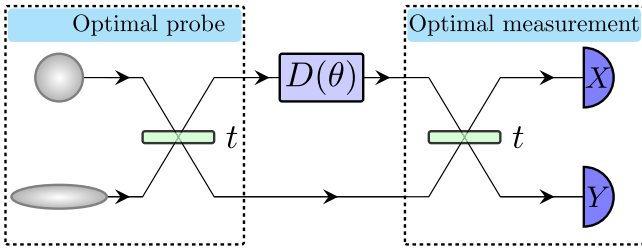


FIG. 4. With one squeezed state and for $w_x < w_y$, the optimal probe configuration is to prepare a Y -squeezed and split it on a beam-splitter with $t = \frac{1}{1+e^{r_2}}$. The optimal measurement is to disentangle the two modes on a second beam-splitter and perform X and Y quadrature measurements on the two outputs which gives the variances in (17).

For $w_y < w_x$, the optimal use of the probe is to set $\phi_2 = 0$ and the optimal measurement is similar to Fig. 4 but with the measurements X and Y swapped. Repeating as before, we get

$$v_x = \frac{e^{-2r_2}}{t} \quad \text{and} \quad v_y = \frac{1}{1-t}, \quad (19)$$

which is optimal when $\frac{1}{1+e^{r_2}} \leq t \leq 1$. In terms of the precisions, we have the relation

$$\frac{e^{-2r_2}}{v_x} + \frac{1}{v_y} \leq 1, \quad (20)$$

which is plotted as the dotted grey line in Fig. 3 for $e^{-2r_2} = 1/4$.

Finally to access the remaining region when $w_x = w_y$, we require $t = \frac{1}{1+e^{r_2}}$ and the squeezing angle ϕ_2 to vary between 0 and $\pi/2$. The optimal measurement is similar to Fig. 4 except that the quadrature measurement angles are set to $\phi_2 + \pi/2$ in the upper arm and ϕ_2 in the lower arm. Each of the measurement carry information on both θ_x and θ_y . The two measurement outcomes, denoted by random variables M_1 and M_2 , follow Gaussian distributions with

$$\text{mean}(M_1) = \sqrt{1-t}(\theta_y \cos \phi_2 - \theta_x \sin \phi_2), \quad (21)$$

$$\text{var}(M_1) = 1, \quad (22)$$

and

$$\text{mean}(M_2) = \sqrt{t}(\theta_y \sin \phi_2 + \theta_x \cos \phi_2), \quad (23)$$

$$\text{var}(M_2) = e^{-2r_2}. \quad (24)$$

With this, we can form two unbiased estimators for θ_x and θ_y :

$$\hat{\theta}_x = \frac{M_2 \cos \phi_2}{\sqrt{t}} - \frac{M_1 \sin \phi_2}{\sqrt{1-t}}, \quad (25)$$

$$\hat{\theta}_y = \frac{M_2 \sin \phi_2}{\sqrt{t}} + \frac{M_1 \cos \phi_2}{\sqrt{1-t}}. \quad (26)$$

The variances of these estimators are

$$\text{var}(\hat{\theta}_x) = \frac{e^{-2r_2} \cos^2 \phi_2}{t} + \frac{\sin^2 \phi_2}{1-t} \quad (27)$$

$$= (1+e^{r_2})e^{-2r_2}(\cos^2 \phi_2 + e^{r_2} \sin^2 \phi_2), \quad (28)$$

and

$$\text{var}(\hat{\theta}_y) = \frac{e^{-2r_2} \sin^2 \phi_2}{t} + \frac{\cos^2 \phi_2}{1-t} \quad (29)$$

$$= (1+e^{r_2})e^{-2r_2}(\sin^2 \phi_2 + e^{r_2} \cos^2 \phi_2), \quad (30)$$

which saturates the bound (16).

B. Example 2: Two equally squeezed state

In our second example, we walk through the derivations of our main result in the special case where the initial resource are two squeezed states having an equal amount of squeezing $r_1 = r_2 = r$. In this case, when $\phi_2 = \phi_1 + \pi/2$, the Holevo-CRB can be simplified to

$$w_x v_x + w_y v_y \geq f_{\text{HCR}} = \min_{\lambda} \{w_x f_x + w_y f_y\}, \quad (31)$$

where

$$f_x := \frac{(1 + \lambda \sqrt{t} e^r)^2 + \lambda^2 (1-t) e^{-2r}}{(\lambda + \sqrt{t} e^{-r})^2}, \quad (32)$$

$$f_y := \frac{(1 + \lambda \sqrt{t} e^r)^2 + \lambda^2 (1-t) e^{-2r}}{(1-t) e^{-2r}}. \quad (33)$$

In general, there is no analytical solution for the optimal value of λ . To see how this leads to the main result in Eq. (10), let us first consider a specific use of the resource by interfering the two squeezed states on a beam splitter with $t = 0.5$ as shown in Fig. 2(a). In this case, the optimal λ that minimizes f_{HCR} is given by $\lambda^* = -e^{-r}(1+\gamma)/\sqrt{2}$ where γ is the positive solution to the quartic equation

$$\frac{w_y}{w_x} \gamma^3 (\gamma - \tanh 2r) + \gamma \tanh 2r - 1 = 0. \quad (34)$$

We can solve some special cases analytically:

$$(w_x = w_y = 1) : v_x + v_y \geq 4e^{-2r} \text{ at } \lambda^* = -\sqrt{2}e^{-r},$$

$$(w_x = 1, w_y = 0) : v_x \geq \frac{1}{\cosh 2r} \text{ at } \lambda^* = \frac{-e^r}{\sqrt{2} \sinh 2r},$$

$$(w_x = 0, w_y = 1) : v_y \geq \frac{1}{\cosh 2r} \text{ at } \lambda^* = \frac{-e^r}{\sqrt{2} \cosh 2r}.$$

$$(35)$$

For other values of w_x/w_y , λ^* can be calculated numerically and several of these bounds are plotted as the dashed lines in Fig. 5 when $e^{-2r} = 1/4$. The envelope of these bounds is defined by the parametric equation $v_x = f_x$ and $v_y = f_y$ for $-\frac{e^r}{\sqrt{2} \sinh 2r} < \lambda < -\frac{e^r}{\sqrt{2} \cosh 2r}$ and by construction can always be reached. This is the precision limit attainable by the probe and is plotted in red in Fig. 5. It is interesting to note that the optimal variance of $v_x = \frac{1}{\cosh 2r}$ can be achieved for any $v_y \geq \frac{\cosh 2r}{\sinh^2 2r}$.

The optimal precision as given by Eq. (10) is plotted in grey in Fig. 5. We see that setting $t = 0.5$ is only optimal when $w_x = w_y$ which gives $v_x = v_y = 2e^{-2r}$ [27]. For every other points on the grey line, a different probe configuration is needed to achieve it. In other words, assigning different weights to the precisions of the two quadratures will require the resource to be used differently. In the extreme case where we are interested in only one quadrature, the optimal scheme

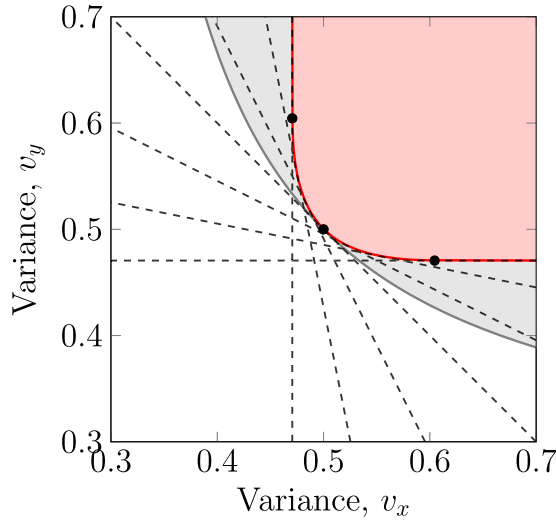


FIG. 5. Precision limits with two 6 dB squeezed resource. Each black dashed line is a Holevo-CRb (31) determined by a value of w_x and w_y for a specific probe where $t = 0.5$. The Holevo-CRb is an attainable bound, which means that for each of this line, there is a measurement that can reach at least one point on it. The three dots corresponds to the three special cases discussed in the main text in Eq. (35). The red line, which is the collection of all the black line bounds, gives the achievable variances for this probe. The grey shaded area, defined by Eq. (38) is the collection of all accessible regions we can attain by varying t . We see that the red region touches the grey line at only one point when $v_x = v_y$. To reach the other points on the grey line, we need to use the resource in a different way with $t \neq 0.5$.

would be to just use one mode to sense the displacement, as in squeezed state interferometry [1–3]. In general, when $w_x \neq w_y$, the optimal way to use the available resource is to mix the two squeezed states on an unbalanced beam-splitter with transmissivity $t^* = \frac{\sqrt{w_y}}{\sqrt{w_x} + \sqrt{w_y}}$. At this value of t , f_{HCR} in Eq. (31) is minimized when $\lambda^* = -e^{-r}/\sqrt{t^*}$ which gives Holevo-CRB as

$$f_{\text{HCR}} = (\sqrt{w_x} + \sqrt{w_y})^2 e^{-2r}. \quad (36)$$

The measurement that saturates this bound is shown in Fig. 6. After the second beam-splitter, the displaced two-mode probe is separated into two independent single-mode probes with displacements $\sqrt{1-t^*}\theta$ and $\sqrt{t^*}\theta$. Measuring X on the first mode and Y on the second gives

$$v_x = \frac{e^{-2r}}{1-t^*} \quad \text{and} \quad v_y = \frac{e^{-2r}}{t^*}. \quad (37)$$

Upon eliminating t^* , we have

$$\frac{1}{v_x} + \frac{1}{v_y} = e^{2r}, \quad (38)$$

which saturates the bound (10). This precision relation quantifies the resource apportioning principle and implies that the quantum resource available through the squeezed states has

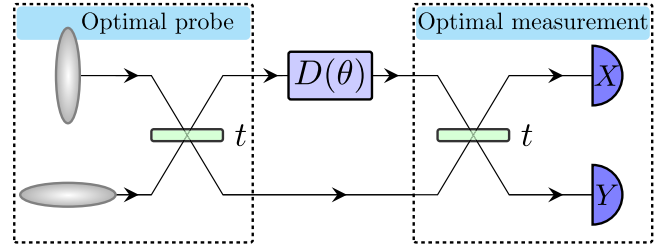


FIG. 6. When $r_1 = r_2$, for a fixed w_x and w_y , the optimal probe that saturates the Holevo-CRb bound is obtained by mixing the two squeezed states on a beam-splitter with t set to $\frac{\sqrt{w_y}}{\sqrt{w_x} + \sqrt{w_y}}$. The optimal measurement is to disentangle the probe into a product of single-mode states and measure X on the first mode and Y on the second mode. This gives the variances in Eq. (37).

to be shared between the two conjugate quadratures [48]. The effects of channel noise and inefficient detectors are presented in Appendix D.

V. DISCUSSIONS AND CONCLUSION

To summarize, we find precision bounds in the simultaneous estimation of two conjugate quadratures. These bounds quantify a resource apportioning principle that limits how much precision is achievable with a given resource. While we restrict to pure states and two-mode states in this work to derive transparent analytical results, our formalism can be generalized to mixed and multimode Gaussian probes. These results can be applied to channel estimation when the amplitude and phase displacements have different strengths. For example, the phase signal can be much weaker than the amplitude signal we are trying to detect. This problem can also be formulated in a resource theory framework [50–55], where squeezing is a resource and passive transformations are free operations. In this framework, the monotone that quantifies the value of the resource will depend on the weights w_x and w_y assigned to each parameter. What *optimal* means must depend on the application which assigns the weights w_x and w_y .

ACKNOWLEDGMENTS

We thank H. Jeng for help in deriving the proofs. This work was supported in part by National Natural Science Foundation of China (91836302, 91736105, 11527808) and National Key Research and Development Program of China (2016YFA0301403). S.M.A. and P.K.L. is supported by the Australian Research Council (ARC) under the Centre of Excellence for Quantum Computation and Communication Technology (CE110001027). Z.Y.O. is supported by US National Science Foundation (Grant No. 1806425).

APPENDIX A: PRELIMINARIES AND NOTATIONS

We introduce some preliminaries and notations that will be used in Appendices B and C to derive the results in the main text. We define the following operators.

$X = a + a^\dagger$	Amplitude quadrature operator
$Y = i(a^\dagger - a)$	Phase quadrature operator
$\Phi(\phi) = \exp(i\phi a^\dagger a)$	Phase shift operator
$D(\theta_x, \theta_y) = \exp\left(\frac{i\theta_y}{2}X - \frac{i\theta_x}{2}Y\right)$	Displacement operator
$S(r) = \exp\left(\frac{r}{2}(a^2 - a^{\dagger 2})\right)$	Squeezing operator
$B(\vartheta) = \exp(\vartheta(a_1^\dagger a_2 - a_1 a_2^\dagger))$	Beam-mixing operator

The beam-splitter transmission is $t = \cos^2 \vartheta$. Some useful elementary relations for single mode operators are listed below.

$$\Phi^\dagger(\phi)D(\theta_x, \theta_y)\Phi(\phi) = D(\theta_x \cos \phi + \theta_y \sin \phi, \theta_y \cos \phi - \theta_x \sin \phi), \quad (\text{A1})$$

$$\frac{\partial}{\partial \theta_x}(\Phi^\dagger(\phi)D(\theta_x, \theta_y)\Phi(\phi))|_{\theta=0} = -\frac{i}{2}X \sin \phi - \frac{i}{2}Y \cos \phi, \quad (\text{A2})$$

$$\begin{aligned} \Phi^\dagger(\phi_1, \phi_2)B_{12}^\dagger(t)D_2(\theta_x, \theta_y)B_{12}(t)\Phi(\phi_1, \phi_2) &= \Phi^\dagger(\phi_1, \phi_2)B_{12}^\dagger(t)D_1(-\sqrt{1-t}\theta_x, -\sqrt{1-t}\theta_y)D_2(\sqrt{t}\theta_x, \sqrt{t}\theta_y)\Phi(\phi_1, \phi_2) \\ &= D_1(-\sqrt{1-t}\theta_x \cos \phi_1 - \sqrt{1-t}\theta_y \sin \phi_1, -\sqrt{1-t}\theta_y \cos \phi_1 + \sqrt{1-t}\theta_x \sin \phi_1) \\ &\quad \otimes D_2(\sqrt{t}\theta_x \cos \phi_2 + \sqrt{t}\theta_y \sin \phi_2, \sqrt{t}\theta_y \cos \phi_2 - \sqrt{t}\theta_x \sin \phi_2), \end{aligned}$$

$$\begin{aligned} \frac{\partial}{\partial \theta_x}(\Phi^\dagger(\phi_1, \phi_2)B_{12}^\dagger(t)D_2(\theta_x, \theta_y)B_{12}(t)\Phi(\phi_1, \phi_2))|_{\theta=0} &= \left(\frac{i}{2}\sqrt{1-t}X_1 \sin \phi_1 + \frac{i}{2}\sqrt{1-t}Y_1 \cos \phi_1\right) + \left(-\frac{i}{2}\sqrt{t}X_2 \sin \phi_2 - \frac{i}{2}\sqrt{t}Y_2 \cos \phi_2\right), \end{aligned} \quad (\text{A7})$$

$$\begin{aligned} \frac{\partial}{\partial \theta_y}(\Phi^\dagger(\phi_1, \phi_2)B_{12}^\dagger(t)D_2(\theta_x, \theta_y)B_{12}(t)\Phi(\phi_1, \phi_2))|_{\theta=0} &= \left(-\frac{i}{2}\sqrt{1-t}X_1 \cos \phi_1 + \frac{i}{2}\sqrt{1-t}Y_1 \sin \phi_1\right) + \left(\frac{i}{2}\sqrt{t}X_2 \cos \phi_2 - \frac{i}{2}\sqrt{t}Y_2 \sin \phi_2\right). \end{aligned} \quad (\text{A8})$$

APPENDIX B: HOLEVO CRAMÉR-RAO BOUND FOR A SINGLE-MODE PROBE

Here, we detail the steps leading to the results for a single mode probe. Starting with the squeezed state $|S(r_1)\rangle = S(r_1)|0\rangle$, we apply a phase rotation ϕ_1 and pass the state through the displacement channel to get the probe

$$D(\theta_x, \theta_y)\Phi(\phi_1)|S(r_1)\rangle.$$

To compute the Holevo-CR bound, we first rotate the probe state by $-\phi_1$. This is done to simplify the computations, it is a unitary transformation which does not change the bound as it can be absorbed as part of the optimal measurement. The rotated probe state is then

$$\begin{aligned} |\psi_\theta\rangle &= \Phi^\dagger(\phi_1)D(\theta_x, \theta_y)\Phi(\phi_1)|S(r_1)\rangle \\ &= D(\theta_x \cos \phi_1 + \theta_y \sin \phi_1, \theta_y \cos \phi_1 - \theta_x \sin \phi_1)|S(r_1)\rangle. \end{aligned}$$

1. Inner products between the probe and its derivatives

The probe state at $\theta = 0$ is

$$|\psi_0\rangle = |S(r_1)\rangle.$$

$$\frac{\partial}{\partial \theta_y}(\Phi^\dagger(\phi)D(\theta_x, \theta_y)\Phi(\phi))|_{\theta=0} = \frac{i}{2}X \cos \phi - \frac{i}{2}Y \sin \phi. \quad (\text{A3})$$

The squeezed state $|S(r)\rangle = S(r)|0\rangle$ has the following expectation values

$$\begin{aligned} \langle S(r)|X|S(r)\rangle &= 0, \quad \langle S(r)|Y|S(r)\rangle = 0, \\ \langle S(r)|X^2|S(r)\rangle &= \exp(-2r), \end{aligned} \quad (\text{A4})$$

$$\langle S(r)|Y^2|S(r)\rangle = \exp(2r), \quad (\text{A5})$$

$$\langle S(r)|XY|S(r)\rangle = i. \quad (\text{A6})$$

Some useful elementary relations for two mode operators are listed below:

Using Eqs. (A2) and (A3), differentiating $|\psi_\theta\rangle$ with respect to θ_x and θ_y , we get

$$|\psi_x\rangle = \left.\frac{\partial}{\partial \theta_x}|\psi_\theta\rangle\right|_{\theta=0} = \left(-\frac{i}{2}X \sin \phi_1 - \frac{i}{2}Y \cos \phi_1\right)|S(r_1)\rangle$$

and

$$|\psi_y\rangle = \left.\frac{\partial}{\partial \theta_y}|\psi_\theta\rangle\right|_{\theta=0} = \left(\frac{i}{2}X \cos \phi_1 - \frac{i}{2}Y \sin \phi_1\right)|S(r_1)\rangle.$$

Using Eqs. (A4) and (A5), the inner products between $|\psi_x\rangle$ and $|\psi_y\rangle$ are

$$\langle \psi_x|\psi_x\rangle = \frac{v_{1y}}{4}, \quad \langle \psi_y|\psi_y\rangle = \frac{v_{1x}}{4},$$

and

$$\langle \psi_x|\psi_y\rangle = \frac{i + \sinh(2r_1)\sin(2\phi_1)}{4} = \frac{\sqrt{v_{1x}v_{1y}}}{4}e^{i\phi},$$

where

$$v_{1y} = e^{-2r_1} \sin^2 \phi_1 + e^{2r_1} \cos^2 \phi_1,$$

$$v_{1x} = e^{-2r_1} \cos^2 \phi_1 + e^{2r_1} \sin^2 \phi_1$$

are the projected variances of the rotated probe on the X and Y quadratures and the angle φ satisfies

$$\cos \varphi = \frac{\sinh(2r_1) \sin(2\phi_1)}{\sqrt{v_{1x}v_{1y}}} = \text{sign}(r_1 \tan \phi_1) \frac{\sqrt{v_{1x}v_{1y} - 1}}{\sqrt{v_{1x}v_{1y}}},$$

$$\sin \varphi = \frac{1}{\sqrt{v_{1x}v_{1y}}}.$$

Together, the inner products between $|\psi_0\rangle$, $|\psi_x\rangle$ and $|\psi_y\rangle$ are

$$\langle \psi_j | \psi_k \rangle = \begin{pmatrix} 1 & 0 & 0 \\ 0 & \frac{1}{4}v_{1y} & \frac{1}{4}\sqrt{v_{1x}v_{1y}}e^{i\varphi} \\ 0 & \frac{1}{4}\sqrt{v_{1x}v_{1y}}e^{-i\varphi} & \frac{1}{4}v_{1x} \end{pmatrix},$$

for $\{j, k\} \in \{0, x, y\}$. Note that the determinant of this matrix is zero because $|\psi_x\rangle$ and $|\psi_y\rangle$ are in fact linearly dependent. To proceed, we introduce a basis and write

$$|\psi_0\rangle = \begin{pmatrix} 1 \\ 0 \end{pmatrix}, \quad |\psi_x\rangle = \frac{\sqrt{v_{1y}}e^{-i\varphi/2}}{2} \begin{pmatrix} 0 \\ 1 \end{pmatrix},$$

$$|\psi_y\rangle = \frac{\sqrt{v_{1x}}e^{i\varphi/2}}{2} \begin{pmatrix} 0 \\ 1 \end{pmatrix}.$$

2. Computation of the Z matrix

In this basis, after applying the conditions

$$\text{tr}\{\rho_\theta \mathcal{X}_j\}|_{\theta=0} = 0, \quad \text{tr}\left\{\frac{\partial \rho_\theta}{\partial \theta_j} \mathcal{X}_k\right\}\Big|_{\theta=0} = \delta_{jk},$$

for $j, k \in \{x, y\}$, the relevant entries for the two matrices \mathcal{X}_x and \mathcal{X}_y are fully determined with

$$\mathcal{X}_x = \begin{pmatrix} 0 & x \\ \bar{x} & . \end{pmatrix}, \quad \mathcal{X}_y = \begin{pmatrix} 0 & y \\ \bar{y} & . \end{pmatrix},$$

where

$$x = \frac{1}{2\sqrt{v_{1y}}} \left(\frac{1}{\cos(\varphi/2)} + i \frac{1}{\sin(\varphi/2)} \right),$$

$$y = \frac{1}{2\sqrt{v_{1x}}} \left(\frac{1}{\cos(\varphi/2)} - i \frac{1}{\sin(\varphi/2)} \right).$$

Substituting this into $Z_\theta[\mathcal{X}]_{jk} := \text{tr}\{\rho_\theta \mathcal{X}_j \mathcal{X}_k\}$, we get

$$Z = \begin{pmatrix} |x|^2 & x\bar{y} \\ \bar{x}y & |y|^2 \end{pmatrix}$$

$$= \begin{pmatrix} v_{1x} & -\sinh(2r_1) \sin(2\phi) + i \\ -\sinh(2r_1) \sin(2\phi) - i & v_{1y} \end{pmatrix},$$

which does not depend on φ .

3. Holevo-CR bound for a fixed weight matrix

With a diagonal weighting matrix

$$W = \begin{pmatrix} w_x & 0 \\ 0 & w_y \end{pmatrix},$$

the function

$$h = \text{Tr}\{W \text{Re}Z\} + \|\sqrt{W} \text{Im}Z \sqrt{W}\|_1$$

$$= w_x v_{1x} + w_y v_{1y} + 2\sqrt{w_x w_y}.$$

Hence the Holevo-CR bound is

$$w_x v_x + w_y v_y \geq w_x v_{1x} + w_y v_{1y} + 2\sqrt{w_x w_y}. \quad (\text{B1})$$

Each value of w_x and w_y in Eq. (B1) restricts the values v_x and v_y can take. For some values of w_x and w_y , we get

$$(w_x = w_y = 1) : v_x + v_y \geq v_{1x} + v_{1y} + 2$$

$$= 2(1 + \cosh 2r_1),$$

$$(w_x = 1, w_y = 0) : v_x \geq v_{1x}, \quad (\text{B2})$$

$$(w_x = 0, w_y = 1) : v_y \geq v_{1y}. \quad (\text{B3})$$

4. Collecting all the bounds with different weighting matrix

To find all the possible values for v_x and v_y , we look for solutions to Eq. (B1) valid for all w_x and w_y . Rearranging Eq. (B1), we have

$$w(v_y - v_{1y}) - 2\sqrt{w} + (v_x - v_{1x}) \geq 0,$$

where $w = w_y/w_x$. This is a quadratic equation in \sqrt{w} and the statement is true for all w if and only if

$$4 - 4(v_y - v_{1y})(v_x - v_{1x}) \leq 0$$

$$\Rightarrow (v_y - v_{1y})(v_x - v_{1x}) \geq 1, \quad (\text{B4})$$

where we already know from Eqs. (B2) and (B3) that $v_x \geq v_{1x}$ and $v_y \geq v_{1y}$.

5. Optimising the rotation angle ϕ

For every rotation angle ϕ , and $v_x > v_{1x}$, relation (B4) gives the smallest value of v_y as

$$v_y = v_{1y} + \frac{1}{v_x - v_{1x}}.$$

Finally, we want to find the rotation angle that minimizes v_y for a fixed v_x . Without any loss of generality, we can consider $r_1 > 0$ so that $v_x > e^{-2r_1}$. Performing the minimisation, we

find

$$v_y^* = \min_{\phi} \left\{ v_{1y} + \frac{1}{v_x - v_{1x}} \right\} \text{ subject to } v_{1x} \leq v_x$$

$$y = \begin{cases} e^{2r_1} + \frac{1}{v_x - e^{-2r_1}} & \text{at } \phi = 0 \\ 2 + 2 \cosh 2r_1 - v_x & \text{at } \phi = \arccos \left(\frac{e^r \sqrt{1+e^{2r_1}-v_x}}{\sqrt{e^{4r}-1}} \right) \\ e^{-2r_1} + \frac{1}{v_x - e^{2r_1}} & \text{at } \phi = \pi/2 \end{cases} \begin{cases} \text{if } e^{-2r_1} \leq v_x < 1 + e^{-2r_1} \\ \text{if } 1 + e^{-2r_1} \leq v_x < 1 + e^{2r_1} \\ \text{if } v_x \geq 1 + e^{2r_1} \end{cases}$$

which is plotted in Fig. 1(c).

APPENDIX C: HOLEVO CRAMÉR-RAO BOUND FOR A TWO-MODE PROBE

This Appendix details the steps leading to the main result for the two-mode probe. An arbitrary two-mode passive linear optical network can be realized by two phase-shifts at the input port, a beam-splitter and a phase-shift at one of the exit port. The phase shift on the exit port can be placed on the mode that is not the probe. Hence this does not have any effect on the estimation precision because it can be undone in the measurement stage. Therefore, starting with the two squeezed states $|S(r_1, r_2)\rangle = S(r_1) \otimes S(r_2)|0, 0\rangle$, it is sufficient to consider just two rotations ϕ_1 and ϕ_2 on each, and mix them through a beam-splitter with splitting ratio t as the most general passive linear operation. The probe state is then

$$D_2(\theta_x, \theta_y)B_{12}(t)\Phi(\phi_1, \phi_2)|S(r_1, r_2)\rangle.$$

To compute the Holevo-CR bound, we first undo the mixing and rotation operation on the probe state by performing $B_{12}(t)$ and $\Phi(\phi_1, \phi_2)$ in reverse. Once again, this is done to simplify the computations, it is a unitary transformation which does not change the bound as it can be absorbed as part of the optimal measurement. The two-mode probe state is then

$$|\psi_{\theta}\rangle = \Phi^{\dagger}(\phi_1, \phi_2)B_{12}^{\dagger}(t)D_2(\theta_x, \theta_y)B_{12}(t)\Phi(\phi_1, \phi_2) \times |S(r_1, r_2)\rangle.$$

1. Inner products between the probe and its derivatives

The probe state at $\theta = 0$ is

$$|\psi_0\rangle = |S(r_1, r_2)\rangle.$$

Using Eqs. (A7) and (A8), we can differentiate $|\psi_{\theta}\rangle$ with respect to θ_x and θ_y to get

$$|\psi_x\rangle = \frac{\partial}{\partial \theta_x} |\psi_{\theta}\rangle \Big|_{\theta=0}$$

$$= \left(\frac{i}{2} \sqrt{1-t} X_1 \sin \phi_1 + \frac{i}{2} \sqrt{1-t} Y_1 \cos \phi_1 \right) |S(r_1, r_2)\rangle$$

$$+ \left(-\frac{i}{2} \sqrt{t} X_2 \sin \phi_2 - \frac{i}{2} \sqrt{t} Y_2 \cos \phi_2 \right) |S(r_1, r_2)\rangle$$

and

$$|\psi_y\rangle = \frac{\partial}{\partial \theta_y} |\psi_{\theta}\rangle \Big|_{\theta=0}$$

$$= \left(-\frac{i}{2} \sqrt{1-t} X_1 \cos \phi_1 + \frac{i}{2} \sqrt{1-t} Y_1 \sin \phi_1 \right) |S(r_1, r_2)\rangle$$

$$+ \left(\frac{i}{2} \sqrt{t} X_2 \cos \phi_2 - \frac{i}{2} \sqrt{t} Y_2 \sin \phi_2 \right) |S(r_1, r_2)\rangle.$$

Using Eqs. (A4) and (A5), the inner products between $|\psi_x\rangle$ and $|\psi_y\rangle$ are

$$\langle \psi_x | \psi_x \rangle = \frac{1-t}{4} v_{1y} + \frac{t}{4} v_{2y},$$

$$\langle \psi_y | \psi_y \rangle = \frac{1-t}{4} v_{1x} + \frac{t}{4} v_{2x},$$

and

$$\langle \psi_x | \psi_y \rangle = \frac{i}{4} + \frac{1-t}{4} \sinh(2r_1) \sin(2\phi_1)$$

$$+ \frac{t}{4} \sinh(2r_2) \sin(2\phi_2)$$

$$= \frac{1-t}{4} \sqrt{v_{1x} v_{1y}} e^{i\varphi_1} + \frac{t}{4} \sqrt{v_{2x} v_{2y}} e^{i\varphi_2},$$

where

$$v_{1y} = e^{-2r_1} \sin^2 \phi_1 + e^{2r_1} \cos^2 \phi_1,$$

$$v_{1x} = e^{-2r_1} \cos^2 \phi_1 + e^{2r_1} \sin^2 \phi_1,$$

$$v_{2y} = e^{-2r_2} \sin^2 \phi_2 + e^{2r_2} \cos^2 \phi_2,$$

$$v_{2x} = e^{-2r_2} \cos^2 \phi_2 + e^{2r_2} \sin^2 \phi_2$$

are the projected variances of the rotated probe on the X and Y quadratures and the angles φ_1 and φ_2 satisfy

$$\cos \varphi_1 = \frac{\sinh(2r_1) \sin(2\phi_1)}{\sqrt{v_{1x} v_{1y}}} = \text{sign}(r_1 \tan \phi_1) \frac{\sqrt{v_{1x} v_{1y} - 1}}{\sqrt{v_{1x} v_{1y}}},$$

$$\sin \varphi_1 = \frac{1}{\sqrt{v_{1x} v_{1y}}},$$

$$\cos \varphi_2 = \frac{\sinh(2r_2) \sin(2\phi_2)}{\sqrt{v_{2x} v_{2y}}} = \text{sign}(r_2 \tan \phi_2) \frac{\sqrt{v_{2x} v_{2y} - 1}}{\sqrt{v_{2x} v_{2y}}},$$

$$\sin \varphi_2 = \frac{1}{\sqrt{v_{2x} v_{2y}}}.$$

Together, the inner products between $|\psi_0\rangle$, $|\psi_x\rangle$, and $|\psi_y\rangle$ are

$$\langle \psi_j | \psi_k \rangle = \begin{pmatrix} 1 & 0 & 0 \\ 0 & \frac{1-t}{4} v_{1y} + \frac{t}{4} v_{2y} & \frac{1-t}{4} \sqrt{v_{1x} v_{1y}} e^{i\varphi_1} + \frac{t}{4} \sqrt{v_{2x} v_{2y}} e^{i\varphi_2} \\ 0 & \frac{1-t}{4} \sqrt{v_{1x} v_{1y}} e^{-i\varphi_1} + \frac{t}{4} \sqrt{v_{2x} v_{2y}} e^{-i\varphi_2} & \frac{1-t}{4} v_{1x} + \frac{t}{4} v_{2x} \end{pmatrix},$$

for $\{j, k\} \in \{0, x, y\}$. To proceed, we introduce a basis and write

$$\begin{aligned} |\psi_0\rangle &= \begin{pmatrix} 1 \\ 0 \\ 0 \end{pmatrix}, \\ |\psi_x\rangle &= \frac{1}{2} \begin{pmatrix} 0 \\ \sqrt{1-t} \sqrt{v_{1y}} e^{-i\varphi_1/2} \\ \sqrt{t} \sqrt{v_{2y}} e^{-i\varphi_2/2} \end{pmatrix}, \\ |\psi_y\rangle &= \frac{1}{2} \begin{pmatrix} 0 \\ \sqrt{1-t} \sqrt{v_{1x}} e^{i\varphi_1/2} \\ \sqrt{t} \sqrt{v_{2x}} e^{i\varphi_2/2} \end{pmatrix}. \end{aligned}$$

2. Computation of the Z matrix

In this basis, after applying the conditions

$$\text{tr}\{\rho_\theta \mathcal{X}_j\}|_{\theta=0} = 0,$$

$$\text{tr}\left\{\frac{\partial \rho_\theta}{\partial \theta_j} \mathcal{X}_k\right\}|_{\theta=0} = \delta_{jk},$$

for $j, k \in \{x, y\}$, we can write the relevant entries for the two matrices \mathcal{X}_x and \mathcal{X}_y as

$$\begin{aligned} \mathcal{X}_x &= \begin{pmatrix} 0 & x_1 e^{i\varphi_1/2} & x_2 e^{i\varphi_2/2} \\ \bar{x}_1 e^{-i\varphi_1/2} & \cdot & \cdot \\ \bar{x}_2 e^{-i\varphi_2/2} & \cdot & \cdot \end{pmatrix}, \\ \mathcal{X}_y &= \begin{pmatrix} 0 & y_1 e^{i\varphi_1/2} & y_2 e^{i\varphi_2/2} \\ \bar{y}_1 e^{-i\varphi_1/2} & \cdot & \cdot \\ \bar{y}_2 e^{-i\varphi_2/2} & \cdot & \cdot \end{pmatrix}, \end{aligned}$$

where the complex entries x_1 , x_2 , y_1 , and y_2 must satisfy the constraints

$$\sqrt{1-t} \sqrt{v_{1y}} \text{Re}\{x_1\} + \sqrt{t} \sqrt{v_{2y}} \text{Re}\{x_2\} = 1, \quad (\text{C1})$$

$$\sqrt{1-t} \sqrt{v_{1x}} \text{Re}\{x_1 e^{i\varphi_1}\} + \sqrt{t} \sqrt{v_{2x}} \text{Re}\{x_2 e^{i\varphi_2}\} = 0, \quad (\text{C2})$$

$$\sqrt{1-t} \sqrt{v_{1y}} \text{Re}\{y_1\} + \sqrt{t} \sqrt{v_{2y}} \text{Re}\{y_2\} = 0, \quad (\text{C3})$$

$$\sqrt{1-t} \sqrt{v_{1x}} \text{Re}\{y_1 e^{i\varphi_1}\} + \sqrt{t} \sqrt{v_{2x}} \text{Re}\{y_2 e^{i\varphi_2}\} = 1. \quad (\text{C4})$$

Substituting this into $Z_\theta[\mathcal{X}]_{jk} := \text{tr}\{\rho_\theta \mathcal{X}_j \mathcal{X}_k\}$, we get

$$Z = \begin{pmatrix} |x_1|^2 + |x_2|^2 & x_1 \bar{y}_1 + x_2 \bar{y}_2 \\ \bar{x}_1 y_1 + \bar{x}_2 y_2 & |y_1|^2 + |y_2|^2 \end{pmatrix}.$$

3. Computation for the Holevo-CR bound

With a diagonal weighting matrix

$$W = \begin{pmatrix} w_x & 0 \\ 0 & w_y \end{pmatrix},$$

the function h can be written as

$$\begin{aligned} h &= \text{Tr}\{W \text{Re}Z\} + \|\sqrt{W} \text{Im}Z \sqrt{W}\|_1 \\ &= w_x \underbrace{(|x_1|^2 + |x_2|^2)}_{f_x} + w_y \underbrace{(|y_1|^2 + |y_2|^2)}_{f_y} \\ &\quad + 2 \sqrt{w_x w_y} \text{Abs}\left\{\underbrace{\text{Im}\{x_1 \bar{y}_1 + x_2 \bar{y}_2\}}_g\right\}. \end{aligned} \quad (\text{C5})$$

The Holevo-CR bound is obtained by the following minimisation

$$w_x v_x + w_y v_y \geq f_{\text{HCR}} := \min_{x_1, x_2, y_1, y_2} h$$

subject to the four constraints (C1)–(C4). When the probe parameters r_1 , r_2 , ϕ_1 , ϕ_2 , and t as well as the weights w_x and w_y are specified, this is an instance of a semidefinite programme which can be solved efficiently using numerical methods. Furthermore, every semidefinite programme has a dual problem which can be used to verify the solution. The minimum point occurs when $g = 0$ at which we obtain a solution for the extremal point as $v_x = f_x$ and $v_y = f_y$. The locus of the extremal points (v_x, v_y) as we vary the ratio w_x/w_y from 0 to infinity gives the boundary of the accessible region for a specified probe. To find the optimal use of a given resource characterized by r_1 and r_2 , we need to further minimize f_{HCR} over the parameters ϕ_1 , ϕ_2 and t . This is what we have done to plot Fig. 2 of the main text.

While solving the semidefinite programme can give us numerical solutions, we can also solve the minimisation problem by solving for the Karush-Kuhn-Tucker conditions for optimality.

4. Proof of main result

In what follows, we provide a proof of our main result. We break up the proof into four steps. First, we prove that h is minimized when $g = 0$. Second, we provide numerical evidence that f_{HCR} is minimized when ϕ_1 and ϕ_2 are either 0 or $\pi/2$. Third, we compute the Holevo-CR bound for a fixed t . Lastly, we vary t to find all the accessible values for v_x and v_y .

Step 1: h is minimized when $g = 0$

We claim that h in Eq. (C5) is minimized when $g = 0$. To proof this claim, we first introduce the rescaled variables

$$\mathbf{x}_1 = \sqrt{w_x} x_1, \quad \mathbf{x}_2 = \sqrt{w_x} x_2, \quad \mathbf{y}_1 = \sqrt{w_y} y_1, \quad \mathbf{y}_2 = \sqrt{w_y} y_2.$$

In the rescaled variables, function to be minimized Eq. (C5) can be written as

$$\begin{aligned} h &= |\mathbf{x}_1|^2 + |\mathbf{x}_2|^2 + |\mathbf{y}_1|^2 + |\mathbf{y}_2|^2 + 2 \text{Abs}\{\text{Im}\{\mathbf{x}_1 \bar{\mathbf{y}}_1 + \mathbf{x}_2 \bar{\mathbf{y}}_2\}\} \\ &= \max\{|\vec{\mathbf{x}} + \vec{\mathbf{y}}|^2, |\vec{\mathbf{x}} - \vec{\mathbf{y}}|^2\}, \end{aligned}$$

where

$$\begin{aligned}\vec{x} &= (\text{Re } x_1 \text{ Im } x_1 \text{ Re } y_2 \text{ Im } y_2)^\top, \\ \vec{y} &= (-\text{Im } y_1 \text{ Re } y_1 \text{ Im } x_2 \text{ - Re } x_2)^\top.\end{aligned}$$

Our claim is then: h is minimized when $\vec{x} \cdot \vec{y} = 0$. We can write the constraints (C1)–(C4) as

$$\begin{pmatrix} c_1 & 0 \\ c_3 & c_4 \end{pmatrix} \begin{pmatrix} \text{Re } x_1 \\ \text{Im } x_1 \end{pmatrix} + \begin{pmatrix} 0 & -c_2 \\ c_6 & -c_5 \end{pmatrix} \begin{pmatrix} \text{Im } x_2 \\ -\text{Re } x_2 \end{pmatrix} = \begin{pmatrix} \sqrt{w_x} \\ 0 \end{pmatrix}, \quad (\text{C6})$$

$$\begin{pmatrix} 0 & c_1 \\ -c_4 & c_3 \end{pmatrix} \begin{pmatrix} -\text{Im } y_1 \\ \text{Re } y_1 \end{pmatrix} + \begin{pmatrix} c_2 & 0 \\ c_5 & c_6 \end{pmatrix} \begin{pmatrix} \text{Re } y_2 \\ \text{Im } y_2 \end{pmatrix} = \begin{pmatrix} 0 \\ \sqrt{w_y} \end{pmatrix}, \quad (\text{C7})$$

where

$$c_1 = \sqrt{1-t} \sqrt{v_{1y}}, \quad c_3 = \sqrt{1-t} \sqrt{v_{1x}} \cos \varphi_1, \quad c_5 = \sqrt{t} \sqrt{v_{2x}} \cos \varphi_2, \quad (\text{C8})$$

$$c_2 = \sqrt{t} \sqrt{v_{2y}}, \quad c_4 = -\sqrt{1-t} \sqrt{v_{1x}} \sin \varphi_1, \quad c_6 = -\sqrt{t} \sqrt{v_{2x}} \sin \varphi_2. \quad (\text{C9})$$

We can invert these equations to find \vec{y} in terms of \vec{x}

$$\begin{aligned}\begin{pmatrix} -\text{Im } y_1 \\ \text{Re } y_1 \end{pmatrix} &= \begin{pmatrix} 0 & c_1 \\ -c_4 & c_3 \end{pmatrix}^{-1} \begin{pmatrix} 0 \\ \sqrt{w_y} \end{pmatrix} - \begin{pmatrix} 0 & c_1 \\ -c_4 & c_3 \end{pmatrix}^{-1} \begin{pmatrix} c_2 & 0 \\ c_5 & c_6 \end{pmatrix} \begin{pmatrix} \text{Re } y_2 \\ \text{Im } y_2 \end{pmatrix}, \\ \begin{pmatrix} \text{Im } x_2 \\ -\text{Re } x_2 \end{pmatrix} &= \begin{pmatrix} 0 & -c_2 \\ c_6 & -c_5 \end{pmatrix}^{-1} \begin{pmatrix} \sqrt{w_x} \\ 0 \end{pmatrix} - \begin{pmatrix} 0 & -c_2 \\ c_6 & -c_5 \end{pmatrix}^{-1} \begin{pmatrix} c_1 & 0 \\ c_3 & c_4 \end{pmatrix} \begin{pmatrix} \text{Re } x_1 \\ \text{Im } x_1 \end{pmatrix},\end{aligned}$$

whenever the matrices $\begin{pmatrix} 0 & c_1 \\ -c_4 & c_3 \end{pmatrix}$ and $\begin{pmatrix} 0 & -c_2 \\ c_6 & -c_5 \end{pmatrix}$ are invertible. This is always true when t is not exactly 0 or 1 in which case we can write $\vec{y} = \mathbb{A}\vec{x} + \vec{b}$, where

$$\begin{aligned}\mathbb{A} &= - \begin{pmatrix} \begin{pmatrix} 0 & c_1 \\ -c_4 & c_3 \end{pmatrix}^{-1} & \mathbb{0} \\ \mathbb{0} & \begin{pmatrix} 0 & -c_2 \\ c_6 & -c_5 \end{pmatrix}^{-1} \end{pmatrix} \begin{pmatrix} \mathbb{0} & \begin{pmatrix} c_2 & 0 \\ c_5 & c_6 \end{pmatrix} \\ \begin{pmatrix} c_1 & 0 \\ c_3 & c_4 \end{pmatrix} & \mathbb{0} \end{pmatrix} \text{ and} \\ \vec{b} &= \begin{pmatrix} \begin{pmatrix} 0 & c_1 \\ -c_4 & c_3 \end{pmatrix}^{-1} & \mathbb{0} \\ \mathbb{0} & \begin{pmatrix} 0 & -c_2 \\ c_6 & -c_5 \end{pmatrix}^{-1} \end{pmatrix} \begin{pmatrix} \sqrt{w_y} \\ \sqrt{w_x} \\ 0 \end{pmatrix}.\end{aligned}$$

Given \vec{x} , the vector \vec{y} is fixed which means we can perform an unconstrained minimisation over \vec{x} only

$$f_{\text{HCR}} = \min_{\vec{x}} \max \{|\vec{x} + \vec{y}|^2, |\vec{x} - \vec{y}|^2\}.$$

Because f_{HCR} is continuous in \vec{x} and bounded below by zero, it has a minimum. To proof our claim we shall show that the alternative statement: “ h is minimized when $\vec{x} \cdot \vec{y} \neq 0$ ” leads to a contradiction. Suppose h is minimized by \vec{x}_* and its corresponding \vec{y}_* such that $\vec{x}_* \cdot \vec{y}_* > 0$. This implies

$$f_{\text{HCR}} = \min_{\vec{x}} |\vec{x} + \vec{y}|^2.$$

However, the function $|\vec{x} + \vec{y}|^2$ attains a minimum of zero when

$$\vec{x}_+ = -(\mathbb{A} + \mathbb{1})^{-1} \vec{b}$$

such that $\vec{y}_+ = -\vec{x}_+$ which implies $\vec{x}_+ \cdot \vec{y}_+ = -|\vec{x}_+|^2 \leq 0$ leading to a contradiction. Following a similar argument, supposing $\vec{x}_* \cdot \vec{y}_* < 0$ also leads to a contradiction. Since the minimum cannot occur when $\vec{x} \cdot \vec{y} \neq 0$, at the minimum point, we must have $\vec{x} \cdot \vec{y} = 0$ which proves our claim. Hence, we

can write the Holevo-CR bound as

$$f_{\text{HCR}} = \min_{\vec{x}} |\vec{x} + \vec{y}|^2, \text{ subject to } \vec{x} \cdot \vec{y} = 0. \quad (\text{C10})$$

Step 2: Numerical evidence that the minimum can be attained when $\phi_1 = 0$ and $\phi_2 = \pi/2$ or $\phi_1 = \pi/2$ and $\phi_2 = 0$

For any given values of r_1, r_2, t, w_x , and w_y , we conjecture that the minimum for h can always be attained when $\phi_1 = 0$ and $\phi_2 = \pi/2$ or when $\phi_1 = \pi/2$ and $\phi_2 = 0$. For each value of ϕ_1 and ϕ_2 we can solve a semi-definite program to find the minimum $f_{\text{HCR}}(\phi_1, \phi_2)$. We can then scan over the angles ϕ_1 and ϕ_2 to look for the minimum f_{HCR} . Doing this, we find that the minimum of f_{HCR} always occur when ϕ_1 and ϕ_2 are equal to either 0 or $\pi/2$. A simulation for a typical setting with $r_1 = 0.35$, $r_2 = 0.69$, $t = 0.4$, $w_x = 0.7$, and $w_y = 0.3$ is shown in Fig. 7(a).

In the special case when $w_x = w_y$, we find that any value every value of ϕ_1 and ϕ_2 satisfying $\phi_2 = \phi_1 + \pi/2$ gives the same optimal f_{HCR} . A typical simulation result is shown in Fig. 7(b).

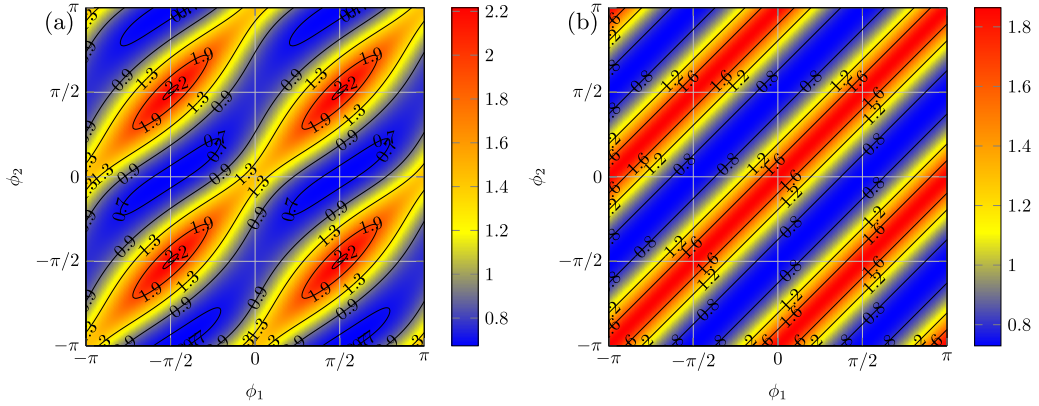


FIG. 7. (a) A typical contour plot of f_{HCR} for a fixed $r_1 = 0.35$, $r_2 = 0.69$, $t = 0.4$, $w_x = 0.7$ and $w_y = 0.3$ as we scan the angles ϕ_1 and ϕ_2 . In this case, f_{HCR} is minimized when $\phi_1 = \pi/2$ and $\phi_2 = 0$. (b) With the same values of r_1 , r_2 and t but for $w_x = w_y = 0.5$, f_{HCR} is now minimized when $\phi_2 = \phi_1 + \pi/2$.

Step 3: Minimizing h for a fixed w_x , w_y , and t , when ϕ_1 and ϕ_2 are equal to 0 or $\pi/2$

When ϕ_1 and ϕ_2 are equal 0 or $\pi/2$ the products $v_{1x}v_{1y} = v_{2x}v_{2y} = 1$ and $\varphi_1 = \varphi_2 = \pi/2$. This simplifies the inner products between the states of interest to

$$\langle \psi_j | \psi_k \rangle = \begin{pmatrix} 1 & 0 & 0 \\ 0 & \frac{1-t}{4}v_{1y} + \frac{t}{4}v_{2y} & \frac{i}{4} \\ 0 & -\frac{i}{4} & \frac{1-t}{4}v_{1x} + \frac{t}{4}v_{2x} \end{pmatrix}.$$

The coefficients $c_3 = c_5 = 0$, $c_4 = -\sqrt{1-t}\sqrt{v_{1x}}$ and $c_6 = -\sqrt{t}\sqrt{v_{2x}}$ in Eqs. (C6) and (C7). The matrix \mathbb{A} and vector \vec{b} relating \vec{y} and \vec{x} are now

$$\mathbb{A} = - \begin{pmatrix} 0 & 0 & 0 & c_6/c_4 \\ 0 & 0 & -c_2/c_1 & 0 \\ 0 & -c_4/c_6 & 0 & 0 \\ c_1/c_2 & 0 & 0 & 0 \end{pmatrix}$$

and

$$\vec{b} = \begin{pmatrix} -\sqrt{w_y}/c_4 \\ 0 \\ 0 \\ -\sqrt{w_x}/c_2 \end{pmatrix}.$$

The relation between the original variables becomes

$$\begin{aligned} \text{Re } x_2 &= \frac{1}{c_2}(1 - c_1 \text{Re } x_1), & \text{Im } x_2 &= -\frac{c_4}{c_6} \text{Im } x_1, \\ \text{Re } y_1 &= -\frac{c_2}{c_1} \text{Re } y_2, & \text{Im } y_1 &= \frac{1}{c_4}(1 - c_6 \text{Re } x_1). \end{aligned}$$

To compute the Holevo-CR bound (C10), we now have to minimize over x_1 and y_2

$$h = w_x f_x + w_y f_y,$$

where

$$\begin{aligned} f_x &= (\text{Re } x_1)^2 + (\text{Im } x_1)^2 + \left(\frac{1 - c_1 \text{Re } x_1}{c_2} \right)^2 + \left(\frac{c_4 \text{Im } x_1}{c_6} \right)^2, \\ f_y &= (\text{Re } y_2)^2 + (\text{Im } y_2)^2 + \left(\frac{1 - c_6 \text{Im } y_2}{c_4} \right)^2 + \left(\frac{c_2 \text{Re } y_2}{c_1} \right)^2 \end{aligned}$$

subject to the condition

$$\begin{aligned} g &= -\text{Im } y_1 \text{Re } x_1 + \text{Re } y_1 \text{Im } x_1 + \text{Im } x_2 \text{Re } y_2 - \text{Re } x_2 \text{Im } y_2 \\ &= \frac{\text{Im } x_1 \text{Re } y_2}{c_1 c_6} - \frac{\text{Re } x_1 \text{Im } y_2}{c_2 c_4} - \frac{\text{Re } x_1}{c_4} - \frac{\text{Im } y_2}{c_2} \\ &= 0. \end{aligned}$$

To find the minimum value of h , we introduce the Lagrangian function

$$\mathcal{L} = h + \lambda g,$$

where λ is the Lagrange multiplier. To find the stationary points for \mathcal{L} we differentiate with respect to x_1 and y_2 and set them to zero:

$$\frac{\partial \mathcal{L}}{\partial \text{Im } x_1} = w_x \left[2\text{Im } x_1 + \frac{2c_4^2}{c_6^2} \text{Im } x_1 \right] + \lambda \left(\frac{\text{Re } y_2}{c_1 c_6} \right) = 0, \quad (\text{C11})$$

$$\frac{\partial \mathcal{L}}{\partial \text{Re } y_2} = w_y \left[2\text{Re } y_2 + \frac{2c_2^2}{c_1^2} \text{Re } y_2 \right] + \lambda \left(\frac{\text{Im } x_1}{c_1 c_6} \right) = 0, \quad (\text{C12})$$

$$\begin{aligned} \frac{\partial \mathcal{L}}{\partial \text{Re } x_1} &= w_x \left[2\text{Re } x_1 - \frac{2c_1}{c_2} \left(\frac{1 - c_1 \text{Re } x_1}{c_2} \right) \right] \\ &\quad - \lambda \left(\frac{\text{Im } y_2}{c_2 c_4} + \frac{1}{c_4} \right) = 0, \end{aligned} \quad (\text{C13})$$

$$\begin{aligned} \frac{\partial \mathcal{L}}{\partial \text{Im } y_2} &= w_y \left[2\text{Im } y_2 - \frac{2c_6}{c_4} \left(\frac{1 - c_6 \text{Im } y_2}{c_4} \right) \right] \\ &\quad - \lambda \left(\frac{\text{Re } x_1}{c_2 c_4} + \frac{1}{c_2} \right) = 0, \end{aligned} \quad (\text{C14})$$

$$\frac{\partial \mathcal{L}}{\partial \lambda} = \frac{\text{Im } x_1 \text{Re } y_2}{c_1 c_6} - \frac{\text{Re } x_1 \text{Im } y_2}{c_2 c_4} - \frac{\text{Re } x_1}{c_4} - \frac{\text{Im } y_2}{c_2} = 0. \quad (\text{C15})$$

From Eqs. (C11) and (C12), we have

$$\begin{aligned} \text{Im } x_1 &= -\frac{\lambda}{2w_x c_1 c_6 (1 + c_4^2/c_6^2)} \text{Re } y_2, \\ \text{Im } x_1 &= -\frac{2w_y c_1 c_6 (1 + c_2^2/c_1^2)}{\lambda} \text{Re } y_2, \end{aligned}$$

which implies either of the two cases.

Case A: $\text{Re } y_2 = \text{Im } x_1 = 0$.

$$\begin{aligned} \text{Case B: } \lambda^2 &= 4w_x w_y c_1^2 c_6^2 \left(1 + \frac{c_2^2}{c_1^2}\right) \left(1 + \frac{c_4^2}{c_6^2}\right) \\ &= 4w_x w_y (c_1^2 + c_2^2)(c_4^2 + c_6^2) \\ \Rightarrow \lambda &= \pm \underbrace{2\sqrt{w_x w_y (c_1^2 + c_2^2)(c_4^2 + c_6^2)}}_{\lambda_0}. \end{aligned}$$

From Eqs. (C13) and (C14), we require

$$\text{Im } y_2 = \frac{2w_x c_4 (c_1^2 + c_2^2) \text{Re } x_1 - 2w_x c_1 c_4 - \lambda c_2^2}{\lambda c_2}, \quad (\text{C16})$$

$$\text{Im } y_2 = \frac{\lambda c_4 \text{Re } x_1 + 2w_y c_2 c_6 + \lambda c_4^2}{2c_2 w_y (c_4^2 + c_6^2)}. \quad (\text{C17})$$

Let's first consider case B. Substituting $\lambda = \pm \lambda_0$ into the two equations above, we get from Eq. (C16)

$$\text{Im } y_2 = \pm \frac{c_4 \sqrt{w_x} \sqrt{c_1^2 + c_2^2}}{\sqrt{w_y} \sqrt{c_4^2 + c_6^2}} \text{Re } x_1 \mp \frac{2w_x c_1 c_4}{\lambda_0 c_2} - c_2$$

and from Eq.(C17)

$$\text{Im } y_2 = \pm \frac{c_4 \sqrt{w_x} \sqrt{c_1^2 + c_2^2}}{\sqrt{w_y} \sqrt{c_4^2 + c_6^2}} \text{Re } x_1 + \frac{2w_y c_2 c_6 \pm \lambda_0 c_4^2}{2c_2 w_y (c_4^2 + c_6^2)}.$$

Except in the special case where

$$\mp \frac{2w_x c_1 c_4}{\lambda_0 c_2} - c_2 = \frac{2w_y c_2 c_6 \pm \lambda_0 c_4^2}{2c_2 w_y (c_4^2 + c_6^2)},$$

case B will not have a solution.

Next we consider case A. Now the constraint (C15) becomes

$$\text{Re } x_1 \text{Im } y_2 + c_2 \text{Re } x_1 + c_4 \text{Im } y_2 = 0. \quad (\text{C18})$$

The remaining task is to solve for $\text{Re } x_1$, $\text{Im } y_2$, and λ from Eqs. (C16), (C17), and (C18). The solution to this is given by

$$\lambda = \frac{2w_x c_4 (c_1^2 + c_2^2) \text{Re } x_1 - 2w_x c_1 c_4}{c_2^2 + c_2 \text{Im } y_2},$$

$$\text{Re } x_1 = -\frac{c_4 \text{Im } y_2}{c_2 + \text{Im } y_2},$$

and $\text{Im } y_2$ is given by the solution to

$$\begin{aligned} -w_x c_4 (c_1^2 + c_2^2) \left(\frac{c_4}{c_2 + \text{Im } y_2}\right)^3 \text{Im } y_2 \\ -w_x c_1 c_4 \left(\frac{c_4}{c_2 + \text{Im } y_2}\right)^2 = w_y c_2 (c_4^2 + c_6^2) \text{Im } y_2 - w_y c_2 c_6. \end{aligned} \quad (\text{C19})$$

When $w_x = 0$, we have

$$\text{Im } y_2 = \frac{c_6}{c_4^2 + c_6^2} = -\frac{\sqrt{t} v_{2x}}{t v_{2x} - t v_{1x} + v_{1x}} =: (\text{Im } y_2)_{\max}.$$

When $w_y = 0$, we have

$$\text{Im } y_2 = -\frac{c_1 c_2}{c_1 + c_4 (c_1^2 + c_2^2)} = -\frac{\sqrt{t} v_{2x}}{t v_{2x} - t v_{1x}} =: (\text{Im } y_2)_{\min}.$$

The Holevo-CR bound becomes

$$\begin{aligned} w_x v_x + w_y v_y &\geq f_{\text{HCR}} = w_x \underbrace{\frac{c_4^2 (\text{Im } y_2)^2 + (1 - c_6 \text{Im } y_2)^2}{(c_2 + \text{Im } y_2)^2}}_{f_x} \\ &\quad + w_y \underbrace{\frac{c_4^2 (\text{Im } y_2)^2 + (1 - c_6 \text{Im } y_2)^2}{c_4^2}}_{f_y}, \end{aligned}$$

where $(\text{Im } y_2)_{\min} \leq \text{Im } y_2 \leq (\text{Im } y_2)_{\max}$ is obtained by solving (C19). Each value of w_x/w_y defines a straight line in the (v_x, v_y) plane. Several of these lines are plotted in Fig. 2(b). The envelope of these lines as we vary w_x/w_y defines the curve parametrized by $v_x = f_x(\text{Im } y_2)$ and $v_y = f_y(\text{Im } y_2)$. This is plotted as the red curve in Fig. 2(b) where the two end points $\text{Im } y_2 = (\text{Im } y_2)_{\min}$ and $\text{Im } y_2 = (\text{Im } y_2)_{\max}$ are indicated by the two black dots.

Step 4: Optimising the splitting ratio t

Next, we want to find the accessible variances as we change the splitting ratio t . Each value of t parametrizes a curve given by

$$\begin{aligned} v_x &= f_x(\text{Im } y_2, t) \\ &= \frac{(1-t)v_{1x}(\text{Im } y_2)^2 + (1 + \sqrt{t} v_{2x} \text{Im } y_2)^2}{(\sqrt{t} v_{2y} + \text{Im } y_2)^2}, \end{aligned} \quad (\text{C20})$$

$$\begin{aligned} v_y &= f_y(\text{Im } y_2, t) \\ &= \frac{(1-t)v_{1x}(\text{Im } y_2)^2 + (1 + \sqrt{t} v_{2x} \text{Im } y_2)^2}{(1-t)v_{1x}}. \end{aligned} \quad (\text{C21})$$

Several of these are plotted as the greenish-blue curves in Fig. 2(c). The envelope of all these curves can be obtained by solving

$$\frac{\partial f_x}{\partial t} \frac{\partial f_y}{\partial t} = \frac{\partial f_x}{\partial \text{Im } y_2} \frac{\partial f_y}{\partial t}.$$

The solution to this is given by

$$\text{Im } y_2 = -\sqrt{\frac{v_{2y}}{t}}.$$

Substituting this into Eqs. (C20) and (C21) gives

$$f_x(t) = \frac{v_{1x}}{1-t}, \quad f_y(t) = \frac{v_{2y}}{t}$$

which can also be written as

$$\frac{v_{1x}}{v_x} + \frac{v_{2y}}{v_y} = 1. \quad (\text{C22})$$

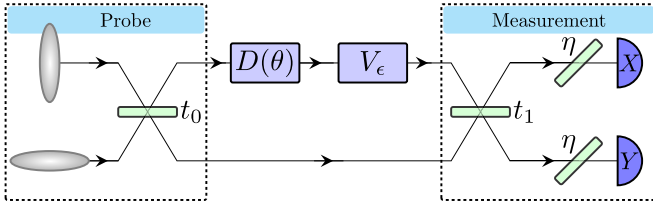


FIG. 8. We model the added noise in the channel by a random gaussian modulation with amplitude V_ϵ in both quadratures. Inefficient detectors are modelled by inserting a beam-splitter with transmissivity η . In the ideal setup with $V_\epsilon = 0$ and $\eta = 1$, the optimal measurement consist of interfering the two beams on a beam-splitter with transmissivity t_1 that depends on t_0 , squeezing level r , and weighting ratios w_x and w_y .

This is plotted as the red enveloping curve in Fig. 2(c). When $\phi_1 = 0$ and $\phi_2 = \pi/2$, Eq. (C22) becomes

$$\frac{e^{-2r_1}}{v_x} + \frac{e^{-2r_2}}{v_y} = 1 \quad (\text{C23})$$

and when $\phi_1 = \pi/2$ and $\phi_2 = 0$, it becomes

$$\frac{e^{-2r_2}}{v_x} + \frac{e^{-2r_1}}{v_y} = 1. \quad (\text{C24})$$

These two bounds are plotted in Fig. 2(d). When $w_x = w_y$, both values of $\phi_1 = 0$ and $\phi_1 = \pi/2$ perform equally well. In this case, as we have seen in Fig. 7(b), any value of $\phi_2 = \phi_1 + \pi/2$ will give the same f_{HCR} . These allow us to access the regions in between the two bounds (C23) and (C24).

APPENDIX D: EFFECT OF CHANNEL NOISE AND LOSSY DETECTORS

In this Appendix, we consider the effects of channel noise and lossy detectors for the two-mode probe example presented in the main text. The channel noise is modelled by adding a random Gaussian noise with variance V_ϵ in both quadratures. The lossy detectors are modelled by adding a beam-splitter with transmissivity η before every detector.

We first consider the case where the first beam-splitter used to mix the probe has a fixed transmissivity $t_0 = 0.5$. The optimal measurement that minimizes the Holevo-CR bound for a given w_x/w_y is shown in Fig. 8 where the transmissivity of the beam-splitter t_1 depends on the ratio of the weights w_x/w_y . It is straightforward to show that the estimation variances with added noise V_ϵ and detector transmissivities η are given by the pair (v_x^*, v_y^*) where

$$v_x^* = \frac{\cosh 2r - 2\sqrt{t_1(1-t_1)} \sinh 2r + (1-t_1)V_\epsilon}{(1-t_1)} + \frac{1-\eta}{\eta(1-t_1)},$$

$$v_y^* = \frac{\cosh 2r - 2\sqrt{t_1(1-t_1)} \sinh 2r + t_1V_\epsilon}{t_1} + \frac{1-\eta}{\eta t_1}.$$

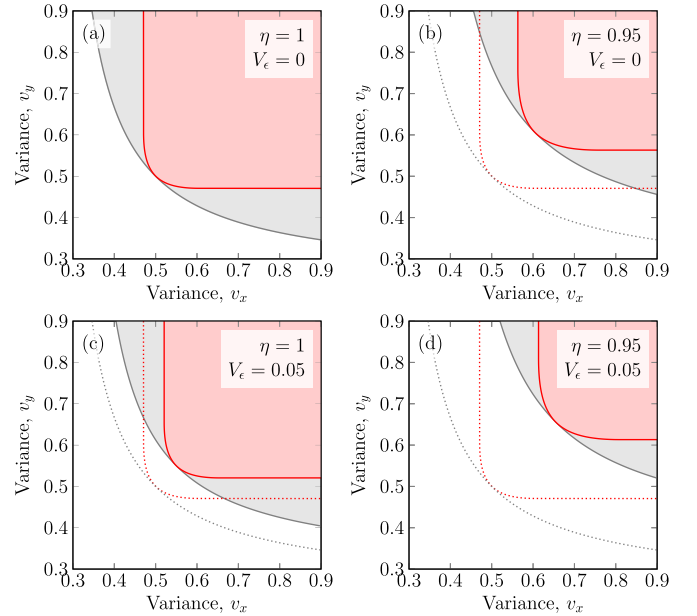


FIG. 9. (a) The accessible regions with two 6 dB squeezed resource ($r = 0.69$) assuming an ideal channel and perfect detectors are shown. The red line is the boundary for the probe with $t_0 = 0.5$ and where the optimal measurement is obtained by varying t_1 . The grey line plots the performance of the optimal probe where $t_0 = t_1 = \frac{\sqrt{w_y}}{\sqrt{w_x} + \sqrt{w_y}}$. In (b), we simulate the effect of lossy detectors with $\eta = 0.95$ which shrinks the accessible region. In (c), we simulate the effect of added noise with $V_\epsilon = 0.05$ —five percent of the vacuum fluctuations. Finally in (d), we consider both channel noise $V_\epsilon = 0.05$ and inefficient detectors $\eta = 0.95$. For comparison, the dotted lines in (b), (c) and (d) are the boundaries for the perfect channel.

The accessible variances for some values of V_ϵ and η are shown as the red shaded region in Fig. 9.

As mentioned in the main text, for the given weights w_x and w_y , the optimal probe is formed by setting $t_0 = \frac{\sqrt{w_y}}{\sqrt{w_x} + \sqrt{w_y}}$. The optimal measurement is to set $t_1 = t_0$ in Fig. 8. It is once again straightforward to show that the estimation variances with added noise V_ϵ and detector transmissivities η are given by the pair (v_x^*, v_y^*) where

$$v_x^* = \frac{\eta(e^{-2r} + (1-t_0)V_\epsilon) + 1 - \eta}{\eta(1-t_0)},$$

$$v_y^* = \frac{\eta(e^{-2r} + t_0V_\epsilon) + 1 - \eta}{\eta t_0}.$$

The accessible variances for some values of V_ϵ and η are shown as the grey shaded region in Fig. 9.

[1] C. M. Caves, Quantum-mechanical noise in an interferometer, *Phys. Rev. D* **23**, 1693 (1981).

[2] M. Xiao, L.-A. Wu, and H. J. Kimble, Precision Measurement Beyond the Shot-Noise Limit, *Phys. Rev. Lett.* **59**, 278 (1987).

[3] P. Grangier, R. E. Slusher, B. Yurke, and A. LaPorta, Squeezed-Light-Enhanced Polarization Interferometer, *Phys. Rev. Lett.* **59**, 2153 (1987).

[4] G. Mauro D'Ariano, P. Lo Presti, and M. G. A. Paris, Using Entanglement Improves the Precision of Quantum Measurements, *Phys. Rev. Lett.* **87**, 270404 (2001).

[5] A. Fujiwara, Quantum channel identification problem, *Phys. Rev. A* **63**, 042304 (2001).

[6] D. G. Fischer, H. Mack, M. A. Cirone, and M. Freyberger, Enhanced estimation of a noisy quantum channel using entanglement, *Phys. Rev. A* **64**, 022309 (2001).

[7] M. Sasaki, M. Ban, and S. M. Barnett, Optimal parameter estimation of a depolarizing channel, *Phys. Rev. A* **66**, 022308 (2002).

[8] A. Fujiwara and H. Imai, Quantum parameter estimation of a generalized pauli channel, *J. Phys. A: Math. Gen.* **36**, 8093 (2003).

[9] M. A. Ballester, Estimation of unitary quantum operations, *Phys. Rev. A* **69**, 022303 (2004).

[10] V. Giovannetti, S. Lloyd, and L. Maccone, Quantum-enhanced measurements: Beating the standard quantum limit, *Science* **306**, 1330 (2004).

[11] M. G. Genoni, M. G. A. Paris, G. Adesso, H. Nha, P. L. Knight, and M. S. Kim, Optimal estimation of joint parameters in phase space, *Phys. Rev. A* **87**, 012107 (2013).

[12] L. Rigovacca, A. Farace, L. A. M. Souza, A. De Pasquale, V. Giovannetti, and G. Adesso, Versatile gaussian probes for squeezing estimation, *Phys. Rev. A* **95**, 052331 (2017).

[13] M. Bradshaw, S. M. Assad, and P. K. Lam, A tight Cramér-Rao bound for joint parameter estimation with a pure two-mode squeezed probe, *Phys. Lett. A* **381**, 2598 (2017).

[14] M. Bradshaw, P. K. Lam, and S. M. Assad, Ultimate precision of joint quadrature parameter estimation with a gaussian probe, *Phys. Rev. A* **97**, 012106 (2018).

[15] Y. Liu, J. Li, L. Cui, N. Huo, S. M. Assad, X. Li, and Z. Y. Ou, Loss-tolerant quantum dense metrology with $SU(1,1)$ interferometer, *Opt. Express* **26**, 27705 (2018).

[16] J. Li, Y. Liu, L. Cui, N. Huo, S. M. Assad, X. Li, and Z. Y. Ou, Joint measurement of multiple noncommuting parameters, *Phys. Rev. A* **97**, 052127 (2018).

[17] P. Gupta, B. L. Schmittberger, B. E. Anderson, K. M. Jones, and P. D. Lett, Optimized phase sensing in a truncated $su(1,1)$ interferometer, *Opt. Express* **26**, 391 (2018).

[18] J. Aasi, J. Abadie, B. P. Abbott, R. Abbott, T. D. Abbott, M. R. Abernathy, C. Adams, T. Adams, P. Addesso, R. X. Adhikari *et al.*, Enhanced sensitivity of the ligo gravitational wave detector by using squeezed states of light, *Nat. Photonics* **7**, 613 (2013).

[19] H. Grote, K. Danzmann, K. L. Dooley, R. Schnabel, J. Slutsky, and H. Vahlbruch, First Long-Term Application of Squeezed States of Light in a Gravitational-Wave Observatory, *Phys. Rev. Lett.* **110**, 181101 (2013).

[20] E. Arthurs and J. L. Kelly, On the simultaneous measurement of a pair of conjugate observables, *Bell Syst. Tech. J.* **44**, 725 (1965).

[21] H. P. Yuen, Generalized quantum measurements and approximate simultaneous measurements of noncommuting observables, *Phys. Lett. A* **91**, 101 (1982).

[22] E. Arthurs and M. S. Goodman, Quantum Correlations: A Generalized Heisenberg Uncertainty Relation, *Phys. Rev. Lett.* **60**, 2447 (1988).

[23] K. Duijvenvoorden, B. M. Terhal, and D. Weigand, Single-mode displacement sensor, *Phys. Rev. A* **95**, 012305 (2017).

[24] S. L. Braunstein and H. J. Kimble, Dense coding for continuous variables, *Phys. Rev. A* **61**, 042302 (2000).

[25] J. Zhang and K. Peng, Quantum teleportation and dense coding by means of bright amplitude-squeezed light and direct measurement of a bell state, *Phys. Rev. A* **62**, 064302 (2000).

[26] X. Li, Q. Pan, J. Jing, J. Zhang, C. Xie, and K. Peng, Quantum Dense Coding Exploiting a Bright Einstein-Podolsky-Rosen Beam, *Phys. Rev. Lett.* **88**, 047904 (2002).

[27] S. Steinlechner, J. Bauchrowitz, M. Meinders, H. Munro, W. Jller-Ebhardt, K. Danzmann, and R. Schnabel, Quantum-dense metrology, *Nat. Photonics* **7**, 626 (2013).

[28] C. W. Helstrom, Minimum mean-squared error of estimates in quantum statistics, *Phys. Lett. A* **25**, 101 (1967).

[29] C. W. Helstrom, Quantum detection and estimation theory, *J. Stat. Phys.* **1**, 231 (1969).

[30] A. S. Holevo, Noncommutative analogues of the Cramér-Rao inequality in the quantum measurement theory, in *Proceedings of the Third Japan USSR Symposium on Probability Theory* (Springer, Berlin, Heidelberg, 1976), p. 194; *Probabilistic and Statistical Aspects of Quantum Theory* (Springer, Basel, 2011).

[31] Y. Gao and H. Lee, Bounds on quantum multiple-parameter estimation with gaussian state, *Eur. Phys. J. D* **68**, 1 (2014).

[32] S. L. Braunstein and C. M. Caves, Statistical Distance and the Geometry of Quantum States, *Phys. Rev. Lett.* **72**, 3439 (1994).

[33] A. Fujiwara and H. Nagaoka, Quantum fisher metric and estimation for pure state models, *Phys. Lett. A* **201**, 119 (1995).

[34] H. Yuen and M. Lax, Multiple-parameter quantum estimation and measurement of nonselfadjoint observables, *IEEE Trans. Inform. Theory* **19**, 740 (1973).

[35] V. P. Belavkin, Generalized uncertainty relations and efficient measurements in quantum systems, *Theor. Math. Phys.* **26**, 213 (1976).

[36] A. Fujiwara, Multi-parameter pure state estimation based on the right logarithmic derivative, *Math. Eng. Tech. Rep.* **94**, 1 (1994).

[37] A. Fujiwara, Linear random measurements of two non-commuting observables, *Math. Eng. Tech. Rep.* **94**, 1 (1994).

[38] A. Fujiwara and H. Nagaoka, An estimation theoretical characterization of coherent states, *J. Math. Phys.* **40**, 4227 (1999).

[39] M. G. A. Paris, Quantum estimation for quantum technology, *Int. J. Quantum Inf.* **7**, 125 (2009).

[40] D. Petz and C. Ghinea, Introduction to quantum fisher information, in *Quantum Probability and Related Topics* (World Scientific, Singapore, 2011), Chap. 15, p. 261.

[41] O. E. Barndorff-Nielsen and R. D. Gill, Fisher information in quantum statistics, *J. Phys. A: Math. Gen.* **33**, 4481 (2000).

[42] M. Szczykulska, T. Baumgratz, and A. Datta, Multi-parameter quantum metrology, *Adv. Phys.: X* **1**, 621 (2016).

[43] J. Suzuki, Information geometrical characterization of quantum statistical models in quantum estimation theory, *Entropy* **21**, 703 (2019).

[44] H. Nagaoka, A new approach to Cramér-Rao bounds for quantum state estimation, in *Asymptotic Theory of Quantum*

Statistical Inference, edited by M. Hayashi (World Scientific, Singapore, 2005), p. 100.

[45] M. Hayashi, *Quantum Information An Introduction* (Springer, Berlin, Heidelberg, 2006).

[46] K. Yamagata, A. Fujiwara, and R. D. Gill, Quantum local asymptotic normality based on a new quantum likelihood ratio, *Ann. Stat.* **41**, 2197 (2013).

[47] F. Albarelli, M. Barbieri, M. G. Genoni, and I. Gianani, A perspective on multiparameter quantum metrology: From theoretical tools to applications in quantum imaging, *Phys. Lett. A* **384**, 126311 (2020).

[48] Y. Liu, N. Huo, J. Li, L. Cui, X. Li, and Z. J. Ou, Optimum quantum resource distribution for phase measurement and quantum information tapping in a dual-beam SU(1,1) interferometer, *Opt. Express* **27**, 11292 (2019).

[49] S. Olivares and M. G. A. Paris, Fidelity Matters: The Birth of Entanglement in the Mixing of Gaussian States, *Phys. Rev. Lett.* **107**, 170505 (2011).

[50] M. Idel, D. Lercher, and M. M. Wolf, An operational measure for squeezing, *J. Phys. A: Math. Theor.* **49**, 445304 (2016).

[51] R. Takagi and Q. Zhuang, Convex resource theory of non-gaussianity, *Phys. Rev. A* **97**, 062337 (2018).

[52] F. Albarelli, M. G. Genoni, M. G. A. Paris, and A. Ferraro, Resource theory of quantum non-gaussianity and wigner negativity, *Phys. Rev. A* **98**, 052350 (2018).

[53] B. Yadin, F. C. Binder, J. Thompson, V. Narasimhachar, M. Gu, and M. S. Kim, Operational Resource Theory of Continuous-Variable Nonclassicality, *Phys. Rev. X* **8**, 041038 (2018).

[54] Q. Zhuang, P. W. Shor, and J. H. Shapiro, Resource theory of non-gaussian operations, *Phys. Rev. A* **97**, 052317 (2018).

[55] H. Kwon, K. C. Tan, T. Volkoff, and H. Jeong, Nonclassicality as a Quantifiable Resource for Quantum Metrology, *Phys. Rev. Lett.* **122**, 040503 (2019).